Effect of hydrogel particle mechanical properties on their disintegration behavior using a gastric digestion simulator

Zaitian Wang[a,b], Hiroyuki Kozu[a], Kunihiko Uemura[b],
Isao Kobayashi[b,]*, and Sosaku Ichikawa[a,]*

[a] *Faculty of Life and Environmental Sciences, University of Tsukuba, 1-1-1 Tennodai, Tsukuba, Ibaraki 305-8572, Japan*

[b] *Food Research Institute, NARO, 2-1-12 Kannodai, Tsukuba, Ibaraki 305-8642, Japan*

---

* Corresponding authors.
E-mail addresses: isaok@affrc.go.jp (I. Kobayashi);
sosaku.ichikawa.fn@u.tsukuba.ac.jp (S. Ichikawa).

Abstract

The interest in designing novel foods whose digestibility can be controlled based on life stage and health conditions continues to grow. Physical digestion is important for solid foods as their breakdown and resulting size reduction can promote enzymatic reactions. Our human gastric digestion simulator (GDS) enables the simulation and direct observation of food particle disintegration induced by simulated antrum contraction waves. The objectives of this study were to verify the disintegration performance of the GDS compared with previously reported *in vivo* data and evaluate the effects of the mechanical properties of hydrogel particles on their *in vitro* gastric disintegration behavior. Agar beads with four fracture forces were prepared and mixed with meal containing locust bean gum to adjust viscosity same as their *in vivo* data. The half residence time of intact beads was longer for hard agar beads than for soft agar beads, and a similar disintegration trend to *in vivo* data was obtained. Moreover, as solid food models, 5-mm hydrogel cubes with different fracture stresses and fracture strains were prepared by varying the agar and native type gellan gum concentrations. The hydrogel cubes disintegrated because of fracture and abrasion during *in vitro* gastric digestion in the presence of simulated antrum contraction waves. The degree of hydrogel cube disintegration was affected by their fracture strain rather than their fracture stress and was suppressed when their fracture strain was greater than 30%. Our findings may provide a better understanding of the gastric digestion behavior of solid foods with different mechanical properties.

Keywords: *In vitro* gastric digestion, Hydrogel, Gastric digestion simulator, Antral contraction waves, Mechanical properties, Disintegration behavior

1. Introduction

The stomach plays an important role in the digestion of foods in the human digestive tract. The main functions of the stomach include storage, mixing, disintegration, and emptying. Solid food is mechanically broken down by chewing, roughly reducing its size to <5.0 mm (Jalabert-Malbos et al., 2007). The bolus sent from the esophagus to the stomach is then temporarily stored in the stomach for less than 3 h (Camilleri et al., 1985; Gardner, Ciociola, & Robinson, 2002). The gastric content comprising food particles, digestive fluids, and digestive enzymes is mixed in the presence of peristaltic motion on the gastric wall. The food particles in the gastric content also disintegrate because of physical movements (antral contraction waves, ACWs) and chemical reactions (digestive enzymes, pH). Because of the gastric disintegration process, most of the digesta with particle diameters less than approximately 2 mm is emptied from the antrum of the stomach (Kelly, 1980; Guo et al., 2014). Investigating the disintegration behavior of solid foods during gastric digestion is a key factor in controlling digestibility and the delivery of the nutrients embedded within foods.

There is an increasing demand for food products whose texture is appropriately designed for elderly, obese, and functional dyspepsia patients. The mechanical properties of solid foods, such as hardness and elasticity, are important parameters for controlling food digestibility in the above-mentioned people. The mechanical properties of hydrogels can be readily varied by adjusting the formulation and/or concentration of the gelling agents (e.g., polysaccharides and proteins). Hydrogels are also commonly used as solid food models in oral food processing research. For example, Ishihara et al. (2014) found that the first size reduction of gellan hydrogels was similar for instrumental compression tests using artificial tongue and *in vivo* human tests. Kohyama et al. (2016) also identified that the mechanical properties of different

types of hydrogels had a strong influence on natural eating behaviors during oral processing in humans. However, the effects of the mechanical properties of hydrogels on their disintegration during gastric digestion remain unclear.

Numerous *in vitro* and *in vivo* studies on the gastric digestion of solid foods have been reported over the past two decades (Kong & Singh, 2008; Dupont et al., 2018). The most common *in vivo* method uses magnetic resonance imaging (MRI), which allows rapid measurements of multiple parameters of gastric function in a single scan (Hoad et al., 2015). This *in vivo* method is ideal for studying the gastric digestion of solid foods but has drawbacks such as ethical constraints and in some cases being a burden on subjects. Different *in vitro* digestion models mimicking the gastric digestion process have been proposed as alternatives to *in vivo* methods. A conventional *in vitro* digestion model involves shaking tubes or flasks to mix food particles with artificial digestive fluids containing digestive enzyme(s) (McClements & Li, 2010). However, this model does not evaluate the disintegration of food particles appropriately because ACWs are absent.

In vitro dynamic models that can consider ACWs have been developed since the mid-1990s (Guerra et al., 2012; Dupont et al., 2018). The TNO Gastro-Intestinal Model-1 (TIM-1), developed by Minekus et al. (1995), allows contraction movements of the soft, flexible gastric vessel walls driven by periodically controlled hydrostatic pressure outside the walls. The contraction movement enhances the mixing of the gastric content. The Dynamic Gastric Model (DGM) mechanically processes gastric content through the movement of a piston and barrel simulating the rhythmic ACWs of the human stomach (Vardakou et al., 2011). However, these dynamic digestion models can be expensive for daily use in the food industry. Chen et al. (2016) developed a 'Rope-Driven' *in vitro* Human Stomach Model (RD-IV-HSM), with the aim of

investigating the effects of gastric morphology on digestion behavior. The RD-IV-HSM modeled the whole gastric morphology using a liquid silicone molding process, and the contraction movements by fastening/relaxing ropes wrapped around the antrum of the modeled stomach. The RD-IV-HSM has reproduced the size distribution of a semi-solid meal during the digestion process; however, it was not effective in breaking down larger food particles into the smaller sizes required for gastric emptying (< ~2 mm). An advanced dynamic *in vitro* human stomach (new DIVHS) system based on the RD-IV-HSM has been developed (Wang et al., 2019). The human gastric simulator (HGS) mimics the ACWs using mechanically operated rollers; however, the ACW-induced motion of the gastric contents cannot be directly observed (Kong & Singh, 2008; Dupont et al., 2018). Recently, *in vitro* stomach digestion devices based on a similar concept have also been proposed (Barros et al., 2016; Liu et al., 2019).

Our group has developed an *in vitro* model named the gastric digestion simulator (GDS) that simplifies the major features of the stomach including gastric peristalsis, which mainly progresses in the antrum (distal stomach), and allows operation of quantitatively simulated ACWs and real-time observation of digestion behavior (Kozu et al., 2014). To study physical gastric digestion, Kozu et al. (2015) performed GDS and flask-shaking experiments using agar cubes as a solid food model. It was reported that agar cubes were only broken down in the GDS experiments, which suggests that simulated ACWs contribute to the disintegration of solid foods. However, quantitative evaluations of the physical forces generated by simulated ACWs and the effect of the mechanical properties of solid foods on the disintegration of food particles remain lacking.

In vivo studies focusing on the contraction force and the force experienced by the target solid food particles during gastric digestion have been reported. Vassallo et al. (1992) measured the

112 force generated by ACWs directly using a reaction force catheter. Marciani et al. (2001)
113 observed the degree of gastric disintegration in subjects who ingested agar beads with several
114 different fracture forces using MRI. Kamba et al. (2000) analyzed the absorption of a maker drug
115 in subjects who ingested press-coated Teflon tablets with several different fracture forces.
116 However, the data obtained from these *in vivo* studies varied widely. We believe that the result
117 reported by Marciani et al. (2001) is the most useful because it provided direct observation of
118 food disintegration in the stomach.

119 To verify the disintegration performance of the GDS it is necessary to compare the *in vitro*
120 data obtained from GDS experiments with the above-mentioned *in vivo* data. Additionally, the
121 quantitative impacts of the mechanical properties of solid foods on the disintegration mechanism
122 remain unclear. The first objective of this study was to validate the GDS device for reproducing
123 human gastric disintegration of solid foods using similar food samples (agar beads with a range
124 of fracture forces 0.53–0.90 N in LBG meals) against the *in vivo* data. The second objective was
125 to evaluate the effect of the mechanical properties of hydrogel particles on their disintegration
126 behavior caused by the simulated ACWs of the GDS using 5×5×5 mm hydrogel cubes
127 containing agar or a mixture of agar and native type gellan gum as a model solid food.

128

129 **2. Materials and methods**

130 *2.1. Gastric digestion simulator (GDS)*

131 The GDS used for this study (Kozu et al., 2014) was equipped with a vessel that models the
132 antrum and rollers that generate ACWs, which provide mechanical forces on the gastric contents
133 (Fig. 1a). The speed (2.5 mm/s) and generation frequency (1.5 cycle/min) of the ACWs that act
134 on the sidewalls of the GDS vessel were controlled based on literature data for the ACWs of

135 healthy adults (Sun et al., 1995). The standard values of the ACWs obtained from *in vivo* studies
136 were 1.5–5.0 mm/s and 1–3 cycles/min (Pal et al., 2004; Marciani et al., 2001; Ajaj et al., 2004;
137 Sun et al., 1995). A temperature control unit maintained the temperature inside and around the
138 GDS vessel at normal human body temperature (~37 °C). As shown in Fig. 1b, each roller
139 contains two foam rubber layers with a 12.5-mm thick exterior layer made of ethylene propylene
140 rubber foam (E-4070) and a 2.5-mm-thick interior layer made of polyurethane rubber foam
141 (SM55;) (INOAC CORPORATION, Tokyo, Japan).

142 The contraction force generated by the GDS rollers was measured using manometry, which
143 was conducted using a digital manometer (testo 510, Testo Co., Ltd., Osaka, Japan; Fig. 1c). The
144 maximum pressure (P_{max}) generated in a 26-mm-diameter silicone balloon was measured by
145 placing the manometer at a position where the occluded clearance in the GDS vessel was a
146 minimum. The balloon was also compressed using a texture profile unit (TPU-2C, Yamaden Co.,
147 Ltd., Tokyo, Japan) equipped with a 40-mm-diameter flat cylindrical probe at a deformation
148 speed of 2.5 mm/s. When the balloon was gradually compressed, the maximum force (F_{max})
149 applied to the balloon and P_{max} in the balloon were recorded to analyze the correlation between
150 the values. The F_{max} value was used to express the maximum contraction force generated by the
151 motion of the rollers.

152 The correlation between the contraction force generated in the GDS vessel and P_{max} was
153 analyzed using the texture profile unit and manometry method (Fig. S1). The contraction force
154 was estimated to be 8.5 ± 0.1 N (n = 5) when the minimum clearance between a pair of rollers
155 was 11.2 ± 0.1 mm (n = 10). The estimated contraction force was converted to mechanical stress
156 for comparison with the *in vivo* data reported in previous research. The calculated mechanical
157 stress ranged from 16.0 to 86.3 kPa. Marciani et al. (2001) reported a fracture force of 0.65 N for

158 12.7-mm-diameter agar beads in the human stomach. Kamba et al. (2000) reported a fracture
159 force of 1.89 N for Teflon-coated tablets (7 mm long and 4 mm wide) containing a marker drug
160 that was released only when the tablets received a force greater than its fracture force. These
161 fracture force values obtained from *in vivo* experiments correspond to a range of mechanical
162 stress of 5.1–67.5 kPa. The contraction force value generated in the GDS vessel was therefore
163 compared with these *in vivo* data.

164 *2.2. Composition of simulated digestive fluids*

165 α-Amylase from *Bacillus subtilis* (#10070) (59.3 U/mg) and pepsin from porcine gastric
166 mucosa (#P7000) (714 U/mg) were purchased from Sigma-Aldrich, Inc. (St. Louis, MO, USA).
167 All salts and chemicals used for preparing simulated saliva fluid (SSF) and simulated gastric
168 fluid (SGF) (Table 1) were purchased from Wako Pure Chemical Industries, Ltd. (Osaka, Japan).
169 The compositions of SSF and SGF shown in Table 1 were adopted with slight modification of
170 the SSF and SGF proposed by Minekus et al. (2014). The pH of the SGF used in this study
171 (Table 1) was based on the literature data for the United States Pharmacopeia (USP) dissolution
172 apparatus II (USP 26, 2003), which employs a solution with a pH close to that of the gastric juice
173 secreted in human stomach.

174 *2.3. Comparison of in vitro gastric digestion using GDS and in vivo human gastric digestion*

175 To investigate whether the GDS simulates the disintegration environment of the human
176 stomach, we prepared spherical agar beads whose composition and size were the same as those
177 used for *in vivo* digestion in the human stomach (Marciani et al., 2001) and the bead
178 disintegration patterns for the two experiments were compared. Agar powder (#010-15815) was
179 purchased from Wako Pure Chemical Industries, Ltd. Several agar beads with different agar

concentrations in the range 1.5–3.0 wt% were prepared. The hot agar hydrosol injected into an acrylic template was slowly cooled for 2 h at 8 °C. Locust bean gum (LBG) (#G0753) purchased from Sigma-Aldrich, Inc. was added to the meal so that the viscosity of the meal was matched to that used for the *in vivo* experiments conducted by Marciani et al., 2001. The LBG meal was prepared by dispersing 10.5 g of LBG powder in 1 L of Milli-Q water with vigorous stirring overnight. The viscosity of the prepared LBG meal was 0.06 Pa·s, which is similar to the value previously reported for the *in vivo* experiments (Marciani et al., 2001). The oral phase was not considered because all the agar gel beads ingested by subjects without chewing were intact after swallowing based on the experimental procedure of this *in vivo* human study. Because the capacity of the GDS vessel is approximately 550 mL, our GDS experiments were performed using 10 agar beads, 100 mL of LBG meal, and 330 mL of SGF for 150 min at 37 °C. The number of agar beads that remained intact (N) was counted every 10 min.

2.4. Effect of hydrogel particle mechanical properties on their disintegration in the GDS

2.4.1. Preparation of hydrogel samples

Agar powder (#010-15815) was purchased from Wako Pure Chemical Industries, Ltd. A native-type gellan gum was kindly provided by San-Ei Gen FFI, Inc. (Osaka, Japan). Hydrogels were prepared by dissolution of different concentrations of agar and native-type gellan gum in Milli-Q water using a magnetic stirrer for 30 min at 90 °C, and subsequent cooling of the hydrosol to 8 °C over 2 h. The concentrations of the gelling agents are presented in Table 2.

2.4.2. Measurement of hydrogel mechanical properties

The mechanical properties (fracture stress and fracture strain) of the hydrogel samples were measured using a texture profile unit equipped with a flat cylindrical probe (16 mm diameter).

Hydrogel samples cut into cylinder shapes (16 mm diameter, 10 mm high) were compressed up to 90% deformation at a probe speed of 2.5 mm/s. The mechanical properties of the hydrogel samples prepared in this study are shown in Table S1. Three-dimensional curve fittings of the fracture stress and fracture strain values of the prepared hydrogels were performed using gnuplot software (Geeknet, Inc., Mountain View, CA, USA). The functions presented in Fig. S2 allowed hydrogel samples with arbitrary mechanical properties to be obtained.

2.4.3. In vitro gastric digestion using the GDS

To independently analyze the influence of two mechanical properties (fracture stress and fracture strain) on gastric disintegration, all hydrogel samples were prepared by fixing the fracture stress or fracture strain (Table 2). The hydrogel samples are described relative to the concentrations of agar and native gellan gum that they contain. For example, A0.7G0.6 indicates the hydrogel sample contains 0.7 wt% agar and 0.6 wt% native gellan gum.

The conditions and procedure for the GDS experiments were based on our previous study (Kozu et al., 2014). In brief, 100 g of the hydrogel was shaped into 5-mm cubes. The cubic shape is more realistic than a spherical shape as the masticated food model for *in vitro* gastric digestion experiments. The size of the hydrogel cubes was based on the size of solid particles transferred to the stomach through the esophagus (< ~5.0 mm) (Jalabert-Malbos et al., 2007). The 5×5×5 mm hydrogel cubes containing agar or a mixture of agar and native type gellan gum were mixed with 30 mL of SSF (pH 7, 37 °C) for 2 min to simulate mastication. A total of 260 mL of SGF (pH 1.3, 37 °C) was added to the above mixture, and then the model gastric content was introduced into the GDS vessel. The pH of the above-mentioned gastric content increased to approximately 2.0 during GDS experiments. Each *in vitro* gastric digestion experiment using the GDS was performed at 37 °C for up to 180 min. The progressive speed and generation frequency

of the ACWs of the GDS were set to 2.5 mm/s and 1.5 cycles/min, respectively. The disintegration behavior of the hydrogel cubes in the GDS vessel was monitored and recorded through the transparent window using a digital video camera.

2.4.4. Observation and classification of digested hydrogel particles

At the end of the *in vitro* gastric digestion experiment, the digesta was transferred to the top of a stack of metal mesh sieves with mesh sizes of 0.60, 1.18, 2.36, and 3.35 mm. The hydrogel particles retained in the gastric vessel were carefully rinsed with Milli-Q water. The hydrogel particles on each sieve were gently washed with Milli-Q water to prevent further particle breakdown during the operation. After the washing steps, the metal sieves were wiped to remove the excess water, and each sieve was weighed to evaluate the particle size distribution of the digesta.

2.5. Statistical analysis

The data were analyzed using SPSS Statistic 24 software. One-way analyses of variance were performed to test significant differences in the mechanical properties, the half residence time ($t_{1/2}$), and the ratio of small particles ($0.60 < d \leq 2.36$ mm) to the initial amount of hydrogel particles at $p < 0.05$.

3. Results and discussion

3.1. Comparison of in vitro and in vivo gastric digestion data for agar beads in LBG meals

In vitro gastric digestion experiments on agar beads in LBG meals were conducted using the GDS. The results obtained in this study were compared with the results of *in vivo* human gastric digestion reported by Marciani et al. (2001). The spherical agar beads with different agar

concentrations in the range 1.5–3.0 wt% prepared in this work had a diameter of approximately 13 mm (Fig. 2), which is similar to those used for the *in vivo* study (12.7 mm diameter) and their fracture forces ranged from 0.53 to 0.90 N (Marciani et al., 2001).

The (disintegrated) agar beads after the GDS experiments (150 min) are also shown in Fig. 2. The agar beads with the lowest agar concentration and fracture force were largely disintegrated compared with the agar beads with higher agar concentrations and fracture forces. The beads initially packed near the bottom of the GDS vessel. Four of the beads were compactly aligned at the bottom of the GDS vessel, while the minimum clearance was above 26 mm without contraction of GDS rollers. When the ACWs were generated on the sidewalls of the GDS vessel, the beads present in the occluded area were affected by the compression force and shear force. Fracture of the beads was primarily observed because of the compression force caused by interaction between neighboring beads.

The agar beads that remained intact (N) at a specific digestion time can be estimated using Eq. 1. The parameter k was calculated by carrying out curve fitting using Eq. 1. The half residence time ($t_{1/2}$) of these beads was then calculated using Eq. 2 (Marciani et al., 2001):

$$N = N_0 e^{-kt} \quad (1)$$

$$t_{1/2} = \frac{ln\,2}{k} \quad (2)$$

where N_0 is the initial number of agar beads and t is the time. Eq. 1 was corrected to Eq. 3 below, which subtracted the blank value of the intact bead number because of the geometry of the GDS vessel:

$$N = N_0' e^{-kt} \quad (3)$$

The batch-type process of the GDS used here does not empty the disintegrated particles. Because of the vertical layout of the GDS vessel, at least five agar beads present in the upper region of the

GDS vessel were not compressed by the ACWs, even after disintegration of the beads present at the bottom of the GDS vessel ($N_0' = N_0 - 5$). Fig. S3 depicts the variations of N and the fitting curves for different agar concentrations using Eq. 3. The half residence time of intact beads significantly increased ($p < 0.05$) between the agar concentrations of 1.89 and 2.39 wt% (fracture force of the agar beads between 0.65 and 0.78 N) (Fig. 3a). A similar trend was reported for the *in vivo* human gastric digestion study (Fig. 3b) (Marciani et al., 2001). Although the absolute value of $t_{1/2}$ was different for the GDS and *in vivo* cases, the threshold of the half residence time of the agar beads was the same. This indicates that although replicating the complex movement of the human stomach during food digestion was not fully achieved, the similar trends observed among the GDS and *in vivo* data are useful for investigating the disintegration behavior of solid foods during gastric digestion.

The physical forces generated in the human stomach that contribute to breaking down solid foods are still not fully understood. It is currently believed that three forces are effective for the disintegration of solid food particles in the human stomach: 1) the contraction force generated by ACWs; 2) the shear force generated by changes of the gastric morphology; 3) the shear force generated by the retropulsive fluid flow in the antrum while the pylorus is shut (Faas et al., 2001; Indireshkumar et al., 2000; Marciani et al., 2001). The contraction force generated in the GDS vessel was approximately 8 N higher than that generated in the human stomach (see Sect. 2.1); however, similar agar bead disintegration trends were observed. The findings obtained in this section suggest that the contraction force generated from ACWs in the GDS does not act sufficiently on the agar beads.

The disintegration of the large agar beads was primarily the result of brittle fracture because the disintegrated pieces (e.g. Fig. 2 (d)) could be fit together to restore the original shape (Beer et

al., 2012). For the design of our GDS, it is appropriate to compare the force experienced by the brittle solid food with *in vivo* data rather than the contraction force generated by the ACWs. It is desirable that the contraction force generated by the ACWs in the GDS is adjusted to be the same order as those from the *in vivo* data (e.g., 0.8 N (liquids) and 2.2 N (solids) according to Vassallo et al. (1992)). Therefore, we adjusted the contraction force generated by the ACWs to be <10 N (see Sect. 2.1). As the force acting on the food particles in the stomach is mainly affected by their size, shape, packing, and interactions, it is useful to compare the *in vitro* results with the *in vivo* results reported by Marciani et al. (2001) using similar food samples. Conversely, the contraction force generated by the ACWs of the RD-IV-HSM, which is another *in vitro* gastric model, was 3.37 ± 0.59 N; however, none of the agar beads with fracture forces in the range 0.15–0.65 N fractured during the 1.5 h digestion process (Chen et al., 2016). The study reported that 3.37 N may not sufficiently act on the large particles of agar beads, which was similar to the GDS findings. In comparison, the half residence time of intact beads significantly increased ($p <$ 0.05) when the fracture force of the agar beads was increased from 0.65 N to 0.78 N during both the *in vivo* experiments and the *in vitro* experiments using the GDS as shown in Fig. 3. This implies that most of the compression forces acting on neighboring particles are in the range 0.65–0.78 N (agar conc. 1.89–2.39 wt%). During the GDS digestion process, the contraction force generated by ACWs converts to compression forces acting on some of the neighboring particles, while some particles may escape compression because of slippage caused by their smooth spherical shape. In the case of brittle fracture, the compression forces acting on neighboring particles (0.65–0.78 N) were able to easily breakdown the beads with low fracture forces (< 0.65 N), but had little effect on the beads with high fracture forces (> 0.78 N).

315 Somewhat larger compression forces acting on some neighboring particles may result in the
316 disintegration of the beads with high fracture forces (> 0.78 N).

317 Although replicating the complex movement of the human stomach during food digestion is
318 difficult, these results indicate that the GDS can simulate the disintegration behavior trends of
319 solid foods in the human stomach. Although there are some differences in the absolute half
320 residence time of agar beads with a given fracture force between the *in vitro* and *in vivo* data, the
321 similar trends observed are useful for investigating the disintegration behavior of solid foods
322 during gastric digestion. Of course, the absolute values of the half residence time results for the
323 GDS likely would have been closer to the *in vivo* data if a GDS equipped with emptying and
324 other more complex functions was used.

325 *3.2. Effect of hydrogel mechanical properties on their disintegration in the GDS*

326 *3.2.1. Direct observation of digestion behavior and size distribution of digested particles*

327 The hydrogel samples were initially cut into 5-mm cubes and settled on the bottom of the
328 GDS vessel. The (disintegrated) hydrogel cubes (A1.4, A1.1G0.7, A0.4G1.1) before or after the
329 GDS experiments (180 min) are also shown in Fig. S4. In the case of A1.4, many fractured
330 hydrogel cubes were observed. In the case of A1.1G0.7 and A0.4G1.1, fewer fractured cubes and
331 some small corner or surface pieces caused from slight abrasion were observed. Fig. 4 depicts
332 the gastric content variation observed at the start and the end of *in vitro* gastric digestion using
333 the GDS and the change of particle size distribution during GDS experiments in the case of
334 hydrogel cubes (A1.4, A1.1G0.7, A0.4G1.1) for which the fracture strains were different while
335 the fracture stresses were the same, maintained at ca. 40 kPa (Table 2). Because of the size
336 reduction, small hydrogel particles tended to distribute and pack more densely in the lower

region of the gastric content, resulting in a decrease in the packing height of the hydrogel particles. From the change in packing height shown in Fig. 4 (i, ii), we found that the small particles ($0.60 < d \leq 2.36$ mm) of A1.4 showed more disintegration than A1.1G0.7 and A0.4G1.1 after 180 min. The wet weight of the fraction between 0.60 mm and 2.36 mm increased with time, which corresponds to the size of particles that solid food disintegrated to approximately 1–2 mm in diameter and that were emptied from the pylorus during human digestion (Kelly et al., 1980, Guo et al., 2014). In the case of A1.4, which had a fracture strain of ca. 30%, the weight ratio of the small particles ($0.60 < d \leq 2.36$ mm) to the initial amount of hydrogel particles increased to 22.1 % and the wet weight of the largest fraction ($d > 3.35$ mm) decreased to 74.8 g after 180 min (Fig. 4 (a, iii)). Compared with the result of the flask-shaking experiments (Kozu et al., 2015), the effect of the largest hydrogel particles ($d > 3.35$ mm) breaking down into small particles ($0.60 < d \leq 2.36$ mm) using the GDS is clear.

3.2.2. Relationship between hydrogel mechanical properties and disintegration

Fig. 5 shows the relationship between the mechanical properties of all hydrogel samples and their disintegration using the GDS (n=3). When the fracture strain exceeded the threshold value (between ca. 30% and 40%), the degree of disintegration was markedly reduced: the ratio of small particles ($0.60 < d \leq 2.36$ mm) to the initial amount of hydrogel particles decreased significantly ($p < 0.05$) as described in Fig. 5(a). In the region in which fracture strain is small (ca. 30%), it was found that when fracture stress exceeded a certain value (40–60 kPa), the degree of hydrogel particle disintegration decreased significantly ($p < 0.05$) (Fig. 5(b)). In the region in which fracture strain is large (ca. 40% and 65%), the fracture stress had little influence on disintegration; the ratio of small particles ($0.60 < d \leq 2.36$ mm) to the initial amount of hydrogel particles showed little change ($p > 0.05$) and fracture stress varied from ca. 20 kPa to

60 kPa. These size-reduction trends could also be seen in the gradual increase of the weight ratio of small particles ($0.60 < d \leq 2.36$ mm) to the initial amount of hydrogel particles during GDS digestion experiments (Fig. S5).

3.2.3. Possible mechanisms for the disintegration of hydrogel particles

A possible mechanism for the gastric disintegration of hydrogels with different mechanical properties in GDS experiments is shown schematically in Fig. 6. We assume that there are two types of fracture mechanism (brittle fracture and ductile fracture). Brittle fracture shows no apparent plastic deformation before fracture, while ductile fracture shows an extensive plastic deformation before fracture (Beer et al., 2012). The concept of the brittle-ductile transition of double network hydrogels has been reported as being applicable to various species of polymeric materials. This could explain how the brittle hydrogels change into ductile hydrogels because of increasing the amount of ductile component (Ahmed et al., 2014).

At equivalent fracture strain (ca. 30%), the fracture stress of A1.0, A1.4, A1.7, and A1.9 increased with agar concentration. Measurement of the mechanical properties of these hydrogel samples showed the typical stress-strain curves for brittle materials (data not shown). The key factor determining the disintegration is the fracture stress (σ_f) compared with the compression stress acting on neighboring hydrogel particles (σ_a). Guo et al. (2015) investigated the disintegration of whey protein emulsion gels with different fracture forces (soft and hard gels) using HGS and showed that the soft gel broke down faster than the hard one. In our experiments, when the fracture stress exceeded a threshold (between 40 kPa and 60 kPa), the degree of hydrogel particle disintegration markedly decreased (Fig. 5(b)). The compression force acting on neighboring hydrogel particles can be estimated at approximately 1.0–1.5 N calculated from the above-mentioned threshold and the contact area of the hydrogel samples (25 mm^2: surface area

383 of one face of a 5-mm hydrogel particle cube). A similar disintegration pattern was obtained in
384 the experiments with agar beads in LBG meals (see Sect. 3.1), the difference in the absolute
385 value of the compression force acting on neighboring hydrogel particles may be due to the
386 different sample shapes (sphere or cube).

387 However, in the case of samples that had a fracture strain above 40%, the influence of
388 fracture stress on disintegration was hardly observed. The hydrogel samples showed the typical
389 stress-strain curves for ductile materials (data not shown) and could sustain an extensive plastic
390 deformation without fracture. Observation after 180 min of GDS digestion (e.g. Fig. S4(c))
391 showed that deformation because the ACWs did not exceed the maximum plastic deformation of
392 the ductile hydrogel particles and that only slight abrasion of the surface or corners occurred.

393

394 **4. Conclusions**

395 Based on the comparison of the GDS results and *in vivo* data (Marciani et al., 2001) using
396 agar beads with different fracture forces in LBG meals, we concluded that the fracture of solid
397 foods caused by the simulated ACWs of the GDS was comparable to that of the human stomach.
398 Our GDS results demonstrated that two fracture mechanisms (brittle fracture and ductile
399 fracture) occurred for hydrogel cubes during gastric digestion. In the case of the low fracture
400 strain hydrogels, the degree of hydrogel disintegration was affected by their fracture stress and
401 was decreased when their fracture stress was greater than a threshold value because mainly
402 brittle fracture occurred. In the case of the high fracture strain hydrogels, little effect of fracture
403 stress on disintegration was found because ductile fracture did not occur when there was
404 insufficient plastic deformation. This study provides useful insights for understanding the gastric

digestion behavior of food hydrogels with different mechanical properties and better design of novel solid foods whose digestibility can be controlled based on life stage and health conditions.

Declaration of interests

None.

Acknowledgments

This work was partially supported by a Japan Society Grant-in-Aid for the Promotion of Science (JSPS) 17H01957.

References

Ajaj, W., Goehde, S.C., Papanikolaou, N., Holtmann, G., Ruehm, S.G., Debatin, J.F., et al. (2004). Real time high resolution magnetic resonance imaging for the assessment of gastric motility disorders. *Gut*, *53*, 1256–1261. https://doi.org/10.1136/gut.2003.038588

Ahmed, S., Nakajima, T., Kurokawa, T., Haque, M., & Gong, J.P. (2014). Brittle–ductile transition of double network hydrogels: Mechanical balance of two networks as the key factor. *Polymer*. *55*, 914-923. https://doi.org/10.1016/j.polymer.2013.12.066

Barros, L., Retamal, C., Torres, H., Zúñiga, R. & Troncoso, E. (2016). Development of an *in vitro* mechanical gastric system (IMGS) with realistic peristalsis to assess lipid digestibility. *Food Research International*, *90*, 216-225. https://doi.org/10.1016/j.foodres.2016.10.049

Beer, F., Johnston, R., Dewolf, J., & Mazurek, D. (2012). *Mechanics of Materials*. (6th ed.). New York: McGraw-Hill.

Camilleri, M., Malagelada, J.R., Brown, M.L., Becker, G., & Zinsmeister, A.R. (1985). Relation between antral motility and gastric emptying of solids and liquids in humans. *American Journal of Physiology-Gastrointestinal and Liver Physiology*, *249*, G580-G585. https://doi.org/10.1152/ajpgi.1985.249.5.G580

Chen, L., Xu, Y., Fan, T., Liao, Z., Wu, P., & Wu, X. (2016). Gastric emptying and morphology of a 'near real' *in vitro* human stomach model (RD-IV-HSM). *Journal of Food Engineering*, *183*, 1-8. https://doi.org/10.1016/j.jfoodeng.2016.02.025

Dupont, D., Alric, M., Blanquet-Diot, S., Bornhorst, G., Cueva, C., Deglaire, A., et al. (2018). Can dynamic *in vitro* digestion systems mimic the physiological reality? *Critical Reviews in Food Science and Nutrition, 23*, 1-17. https://doi.org/10.1080/10408398.2017.1421900

Faas, H., Hebbard, G. S., Feinle, C., Kunz, P., Brasseur, J.G., Indireshkumar, K., et al. (2001). Pressure-geometry relationship in the antroduodenal region in humans. *American Journal of Physiology-Gastrointestinal and Liver Physiology*, *281*, G1214-G1220. https://doi.org/10.1152/ajpgi.2001.281.5.G1214

Gardner, J.D., Ciociola, A.A., & Robinson, M. (2002). Measurement of meal-stimulated gastric acid secretion by *in vivo* gastric autotitration. *Journal of Applied Physiology*, *92*, 427–434. https://doi.org/10.1152/japplphysiol.00956.2001

Guerra, A., Etienne-Mesmin, L., Livrelli, V., Denis, S., Blanquet-Diot, S., & Alric, M. (2012). Relevance and challenges in modeling human gastric and small intestinal digestion. *Trends in Biotechnology*, *30*, 591–600. https://doi.org/10.1016/j.tibtech.2012.08.001

Guo, Q., Ye, A., Lad, M., Dalgleish, D., & Singh, H. (2014). Behaviour of whey protein emulsion gel during oral and gastric digestion: effect of droplet size. *Soft Matter*, *10*, 4173-4183. https://doi.org/10.1039/C4SM00598H

Guo, Q., Ye, A., Lad, M., Ferrua, M., Dalgleish, D., & Singh, H. (2015). Disintegration kinetics of food gels during gastric digestion and its role on gastric emptying: an *in vitro* analysis. *Food and Function, 6(3)*, 756-764. https://doi.org/10.1039/c4fo00700j

Hoad, C.L., Parker, H., Hudders, N., Costigan, C., Cox, E.F., Perkins, A.C., et al. (2015). Measurement of gastric meal and secretion volumes using magnetic resonance imaging. *Physics in Medicine and Biology*, *60(3)*, 1367-1383. https://doi.org/10.1088/0031-9155/60/3/1367

Ishihara, S., Isono., M., Nakao., S., Nakauma., M., Funami., T., Hori., K., et al. (2014). Instrumental uniaxial compression test of gellan gels of various mechanical properties using artificial tongue and its comparsion with human oral strategy for the first size redution. *Journal of Texture Studies, 45(5)*, 354-366. https://doi.org/10.1111/jtxs.12080

Indireshkumar, K., Brasseur, J.G., Fass, H., Hebbard, G.S., Kunz, P., Dent, J., et al. (2000). Relative contributions of "pressure pump" and "peristaltic pump" to gastric emptying. *American Journal of Physiology-Gastrointestinal and Liver Physiology*, *278(4)*, G604-G616. https://doi.org/10.1152/ajpgi.2000.278.4.G604

Jalabert-Malbos, M.L., Mishellany-Dutour, A., Woda, A., & Peyron, M.A. (2007). Particle size distribution in the food bolus after mastication of natural foods. *Food Quality and Preference*, *18*, 803-812. https://doi.org/10.1016/j.foodqual.2007.01.010

Kamba, M., Seta, Y., Kusai, A., Ikeda, M., & Nishimura, K. (2000). A unique dosage from to evaluate the mechanical destructive force in the gastrointestinal tract. *International Journal of Pharmaceutics*, *208(1-2)*, 61-70. https://doi.org/10.1016/s0378-5173(00)00552-4

472 Kelly, K.A. (1980). Gastric emptying of liquids and solids: roles of proximal and distal stomach.
473 *American Journal of Physiology-Gastrointestinal and Liver Physiology*, *239*, G71-G76.
474 https://doi.org/10.1152/ajpgi.1980.239.2.G71
475 Kohyama, K., Hayakawa, F., Gao, Z., Ishihara, S., Funami, T., & Nishinari, K. (2016). Natural
476 eating hehavior of two types of hydrocolloid gels as measured by electromyography:
477 Quantitative analysis of mouthful size effects. *Food Hydrocolloids*, *52*, 243-252.
478 https://doi.org/10.1016/j.foodhyd.2015.07.004
479 Kong, F. & Singh, R.P. (2008). A model stomach system to investigate disintegration kinetics of
480 solid foods during gastric digestion. *Journal of Food Science*, *73(5)*, E202-E210.
481 10.1111/j.1750-3841.2008.00745.x
482 Kozu, H., Nakata, Y., Nakajima, M., Neves, M.A., Uemura, K., Sato, S., et al. (2015). Analysis
483 of disintegration of agar gel particles with different textures using gastric digestion
484 simulator. *Japan Journal of Food Engineering*, *16*, 161-166.
485 https://doi.org/10.11301/jsfe.16.161
486 Kozu, H., Nakata, Y., Nakajima, M., Neves, M.A., Uemura, K., Sato, S., et al. (2014).
487 Development of a human gastric digestion simulator equipped with peristalsis function
488 for the direct observation and analysis of the food digestion process. *Food Science and*
489 *Technology Research*, *20*, 225-233. https://doi.org/10.3136/fstr.20.225
490 Liu, W., Fu, D., Zhang, X., Chai, J., Tian, S., & Han, J. (2019). Development and validation of a
491 new artificial gastric digestive system. *Food Research International, 122*, 183-190.
492 https://doi.org/10.1016/j.foodres.2019.04.015
493 Marciani, L., Gowland, P.A., Fillery-Travis, A., Manoj, P., Wright, J., Smith, A., et al. (2001).
494 Assessment of antral grinding of a model solid meal with echo-planar imaging. *American*

Journal of Physiology-Gastrointestinal and Liver Physiology, *280*, G844-G849. https://doi.org/10.1152/ajpgi.2001.280.5.G844

McClements, D. J. & Li, Y. (2010). Review of *in vitro* digestion models for rapid screening of emulsion-based systems. *Food and Function*, *1*, 32-59. https://doi.org/10.1039/c0fo00111b

Minekus, M., Alminger, M., Alvito, P., Ballance, S., Bohn, T., Bourlieu, C., et al. (2014). A standardized static *in vitro* digestion method suitable for food – an international consensus. *Food and Function*, *5*, 1113-1124. https://doi.org/10.1039/c3fo60702j

Minekus, M., Marteau, P., Havenaar, R., & Huis in't Veld, J.H.J. (1995). A multicompartmental dynamic computer-controlled model simulating the stomach and small intestine. *Alternatives to Laboratory Animals*, *23*, 197–209

Pal, A., Indireshkumar, K., Schwizer, W., Abrahamsson, B., Fried, M., & Brasseur, J.G. (2004). Gastric flow and mixing studied using computer simulation. *Proceedings of the Royal Society B: Biological Sciences*, *271(1557)*, 2587-2594. https://doi.org/10.1098/rspb.2004.2886

Sun, W.M., Smout, A., Malbert, C., Edelbroek, M.A., Jones, K., Dent, J., & Horowitz, M. (1995). Relationship between surface electrogastrography and antropyloric pressures, *American Journal of Physiology-Gastrointestinal and Liver Physiology, 268(3)*, G524-G430. https://doi.org/ 10.1152/ajpgi.1995.268.3.G424

United States Pharmacopeia Convention. (2003). The United States Pharmacopeia: USP 26-the National Formulary NF 21 : by authority of the United States Pharmacopeial Convention, Inc., Meeting at Washington, D.C., April 12-16, 2000. Rockville: United States Pharmacopeia Convention.

Vardakou, M., Mercuri, A., Barker, S.A., Craig, D.Q.M. Faulks, R.M., & Wickham, M.S.J. (2011). Achieving antral grinding forces in biorelevant *in vitro* models: comparing the USP Dissolution Apparatus II and the Dynamic Gastric Model with human *in vivo* data. *AAPS PharmSciTech*, *12(2)*, 620–626. https://doi.org/10.1208/s12249-011-9616-z

Vassallo, M.J., Camilleri, M., Prather, C.M., Hanson, R.B., Thomforde, G.M. (1992). Measurement of axial forces during emptying from the human stomach. *American Journal of Physiology-Gastrointestinal and Liver Physiology, 263*, G230-G239. https://doi.org/10.1152/ajpgi.1992.263.2.G230

Wang, J., Wu, P., Liu, M., Liao, Z., Wang, Y., Dong, Z., et al. (2019). An advanced near real dynamic *in vitro* human stomach system to study gastric digestion and emptying of beef stew and cooked rice. *Food and Function*, *10(5)*, 2914-2915. https://doi.org/10.1039/c8fo02586j

Figure captions

Table 1. Composition of simulated salivary fluid (SSF) and simulated gastric fluid (SGF).

Table 2. Mechanical properties of the hydrogel samples containing agar or a mixture of agar and native type gellan gum.

Fig. 1. Contraction force measured in the GDS. (a): Key components of the GDS. (b): Two layered structure of the rollers. (c): Digital manometer with a silicone balloon.

Fig. 2. Photographs showing the appearance of the agar beads before digestion and after 150 min of digestion. **(a)** 1.50 wt% agar. **(b)** 1.89 wt% agar. **(c)** 2.39 wt% agar. **(d)** 3.00 wt% agar.

Fig. 3. Half residence time of the agar beads for four agar concentrations. **(a)** *In vitro* (GDS): n=3 for each agar concentration. **(b)** *In vivo* (Marciani et al., 2001): n=9 for each agar concentration.

Values with different letters are significantly different ($p < 0.05$).

Fig. 4. Direct observation photographs of the hydrogel cubes during GDS digestion experiments. **(a)** A1.4 (fracture stress 39.6 kPa, facture strain 28.9%). **(b)** A1.1G0.7 (fracture stress 40.0 kPa, facture strain 38.1%). **(c)** A0.4G1.1 (fracture stress 37.5 kPa, facture strain 63.9%). **(i)** Hydrogel cubes before digestion. **(ii)** Hydrogel cubes after 180 min of digestion in the GDS. **(iii)** Size distribution change of A1.4, A1.1G0.7 and A0.4G1.1 with digestion time in the GDS.

Fig. 5. Effects of mechanical properties on the gastric disintegration of hydrogel cubes. **(a)** Horizontal axis: fracture strain. **(b)** Horizontal axis: fracture stress (A1.0, A1.4, A1.7, A1.9).

Fig. 6. Mechanisms for the gastric disintegration of hydrogels with different mechanical properties during the GDS experiments. σ_f : fracture stress of hydrogels. σ_a : compression stress acting on neighboring particles.

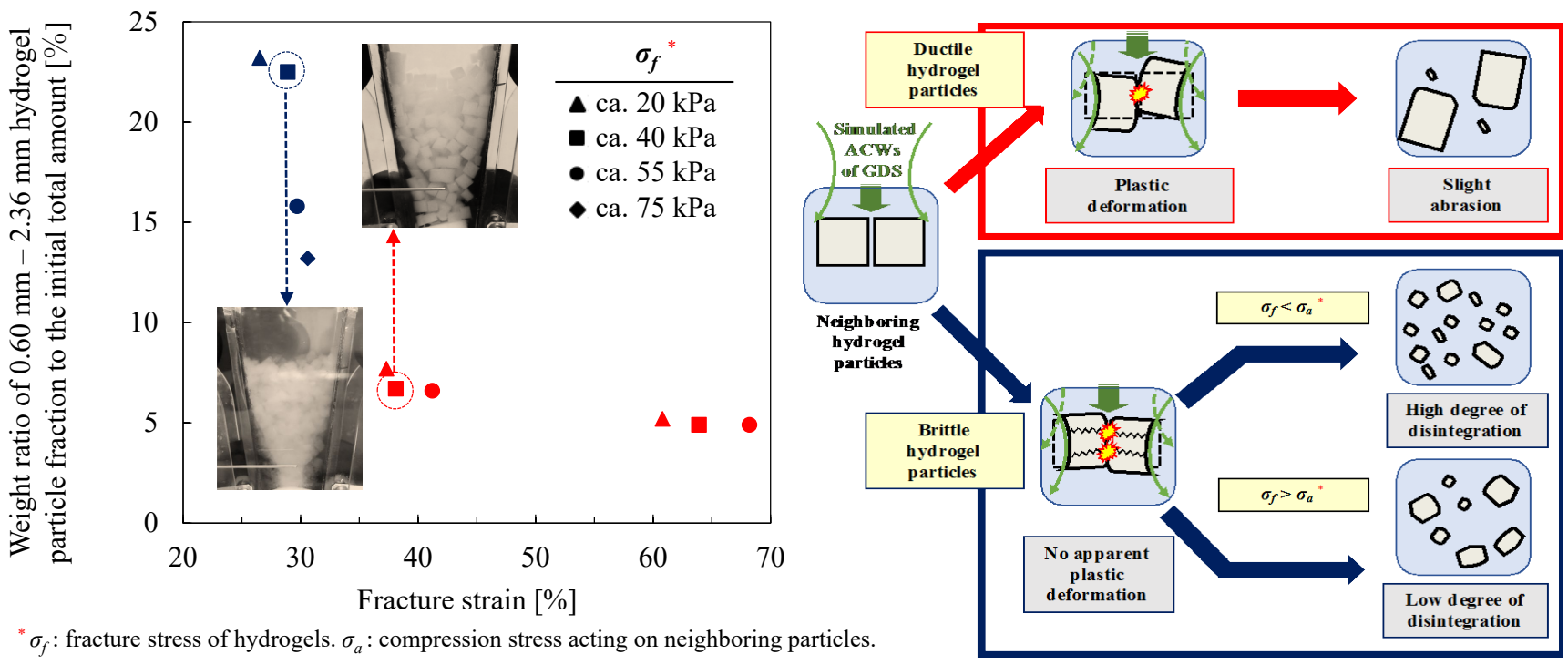

* σ_f : fracture stress of hydrogels. σ_a : compression stress acting on neighboring particles.

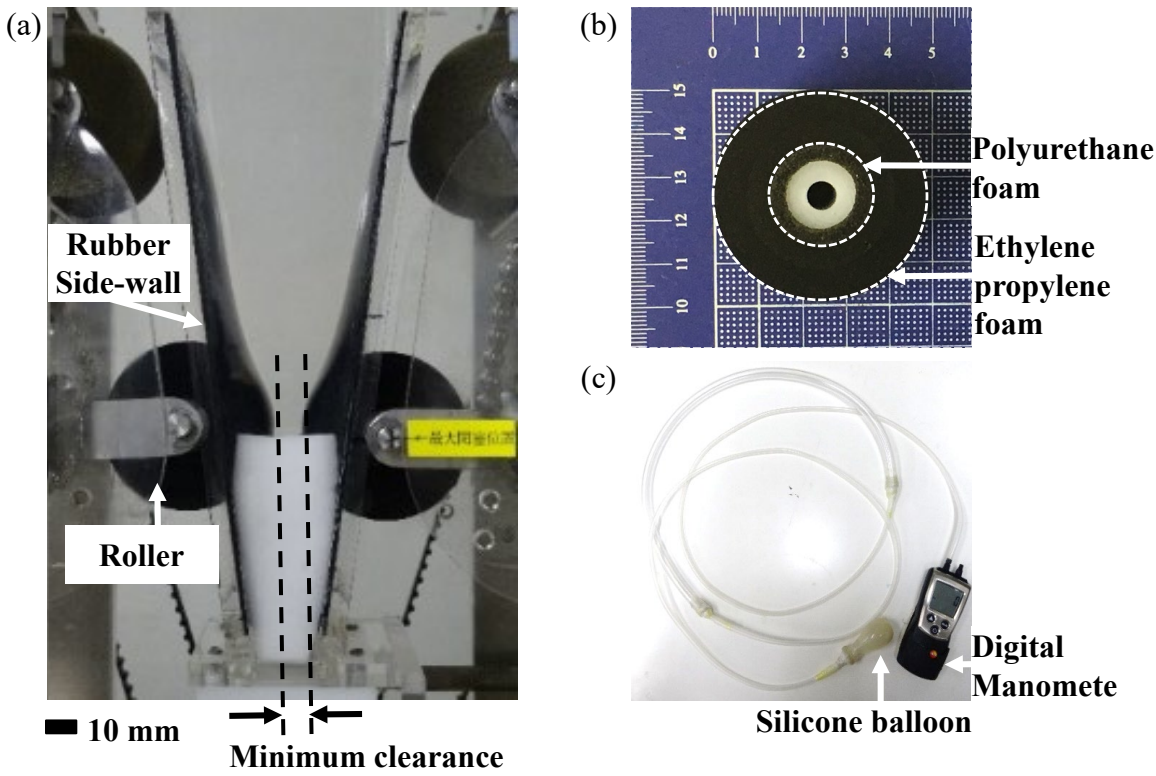
(a)
Rubber
Side-wall
Roller
10 mm
Minimum clearance
(b)
Polyurethane
foam
Ethylene
propylene
foam
(c)
Digital
Manomete
Silicone balloon

Fig. 1

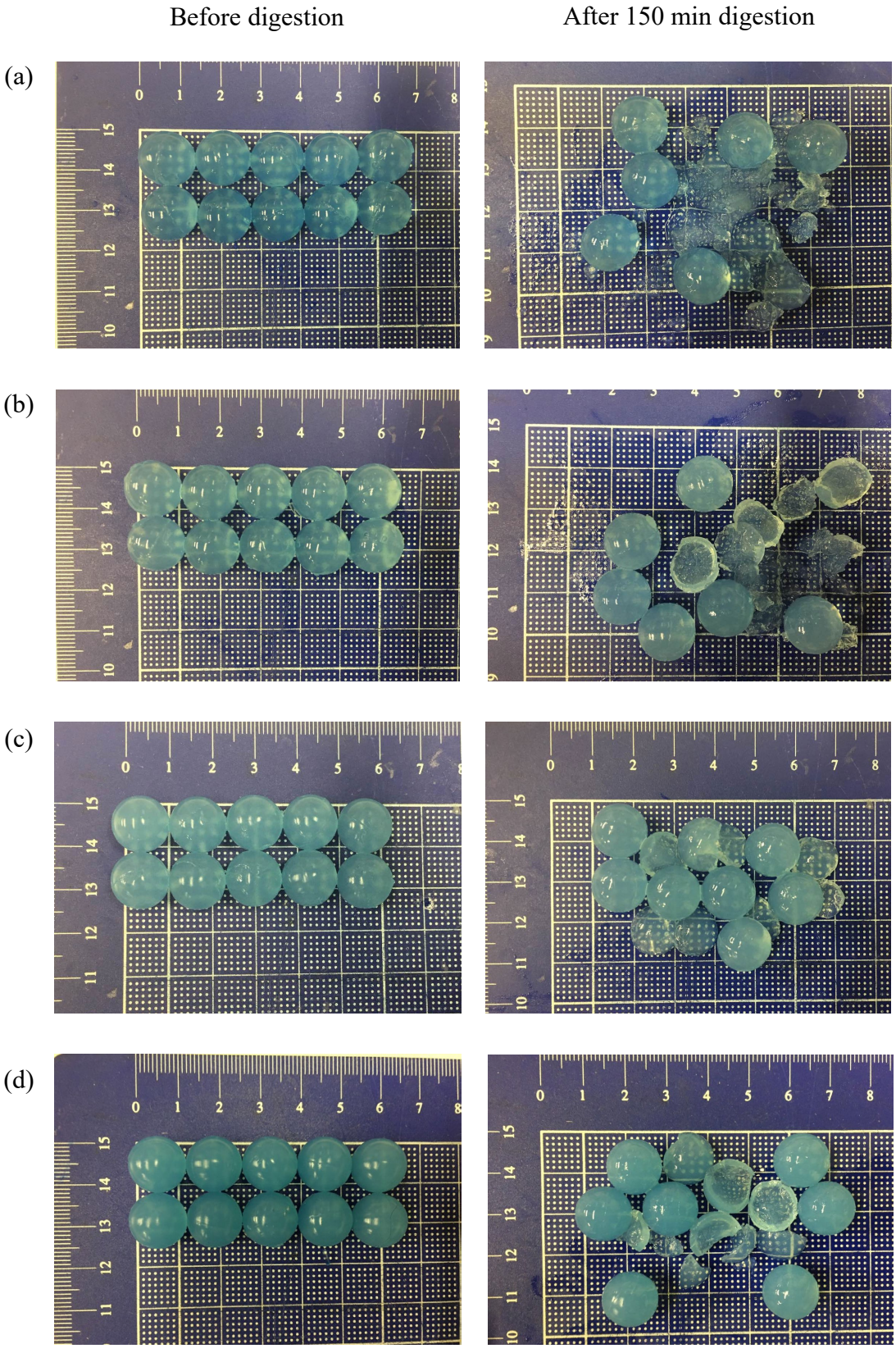

Fig. 2

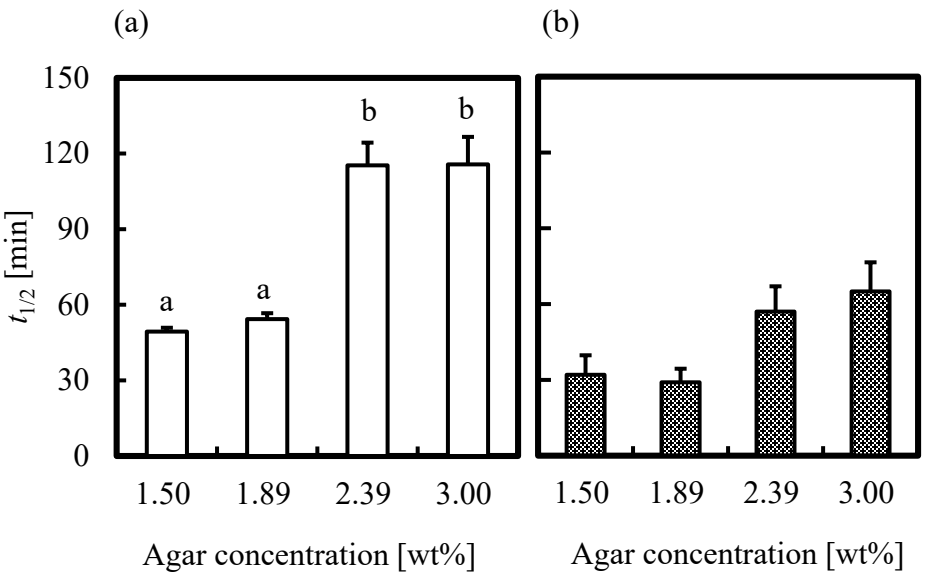
(a)
(b)
150
120
90
60
30
0
$t_{1/2}$ [min]
a
a
b
b
1.50
1.89
2.39
3.00
Agar concentration [wt%]
1.50
1.89
2.39
3.00
Agar concentration [wt%]

Fig. 3

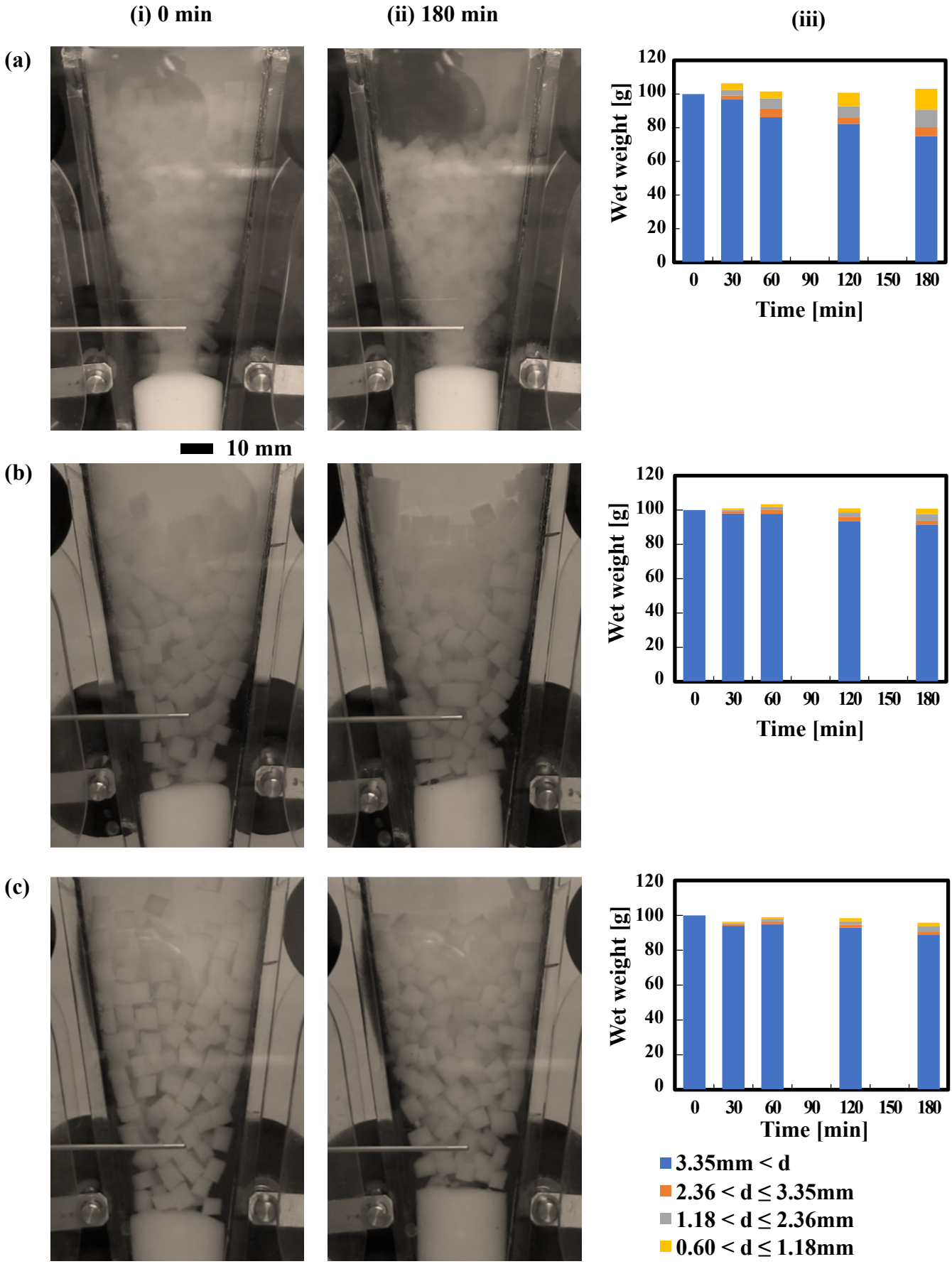
(i) 0 min
(ii) 180 min
(iii)
(a)
(b)
(c)
10 mm
Wet weight [g]
Time [min]
0
20
40
60
80
100
120
0
30
60
90
120
150
180
3.35mm < d
2.36 < d ≤ 3.35mm
1.18 < d ≤ 2.36mm
0.60 < d ≤ 1.18mm

Fig. 4

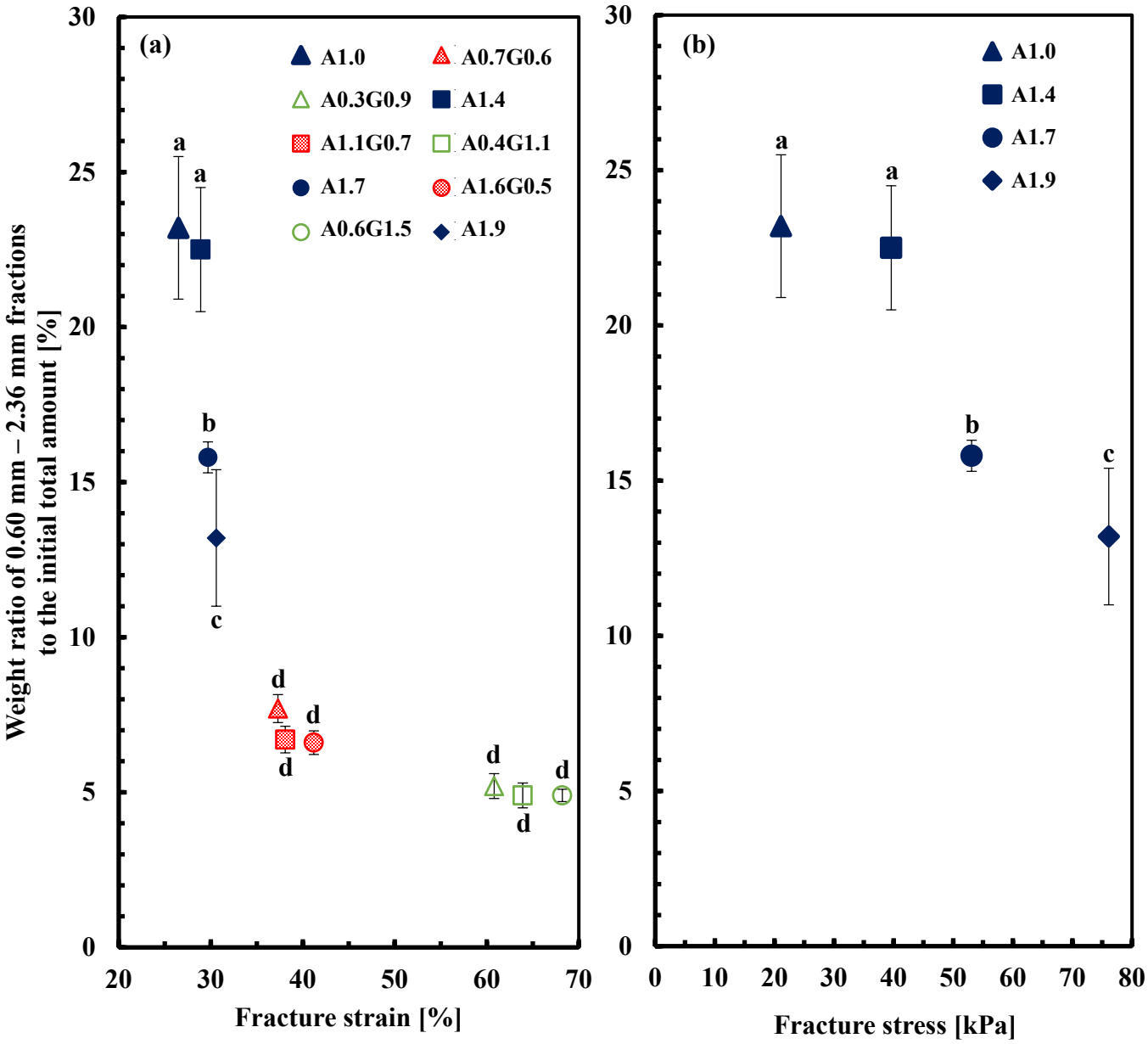
(a)
A1.0
A0.7G0.6
A0.3G0.9
A1.4
A1.1G0.7
A0.4G1.1
A1.7
A1.6G0.5
A0.6G1.5
A1.9
Weight ratio of 0.60 mm – 2.36 mm fractions to the initial total amount [%]
Fracture strain [%]
(b)
A1.0
A1.4
A1.7
A1.9
Fracture stress [kPa]

Fig. 5

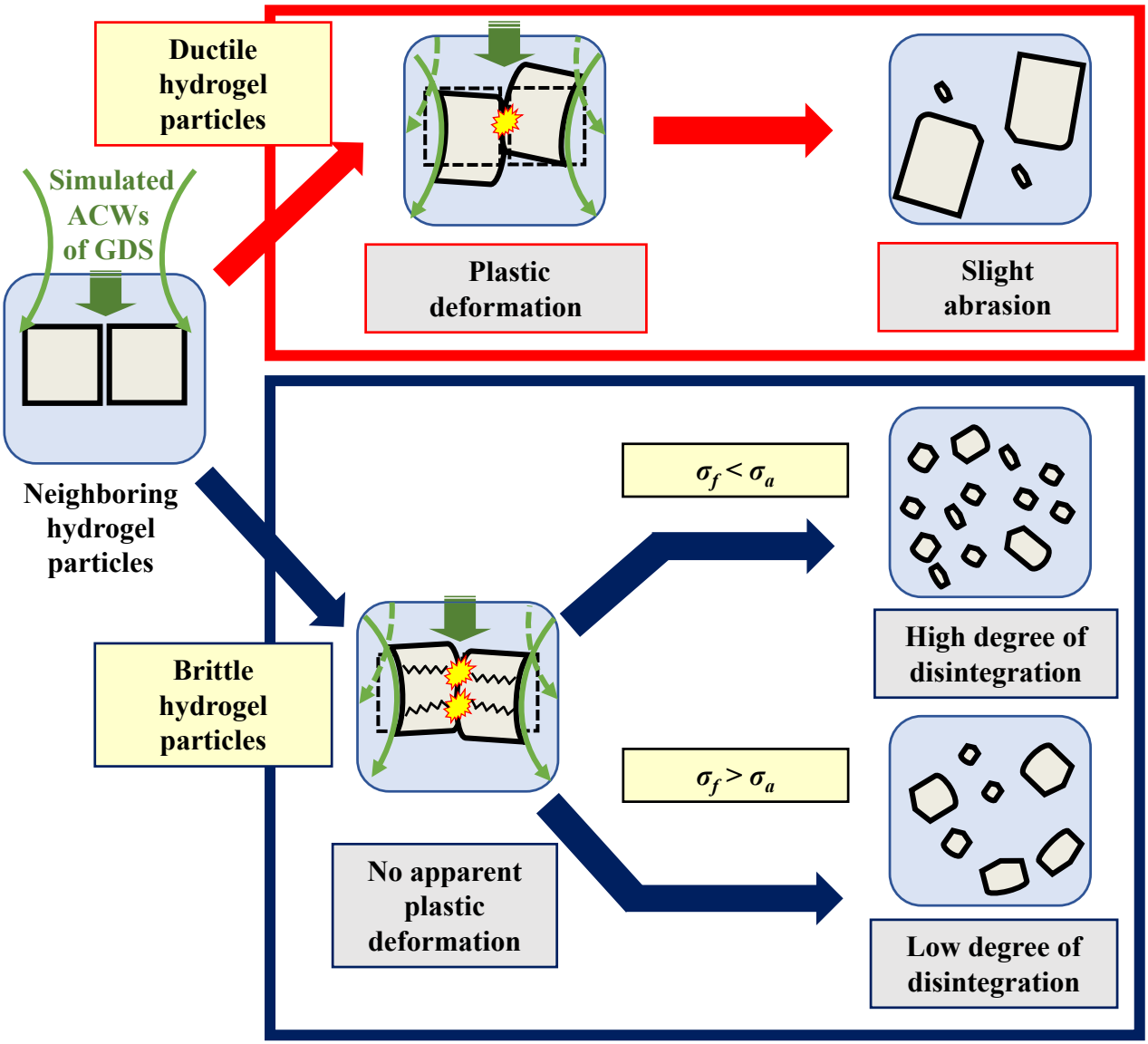
Ductile hydrogel particles
Simulated ACWs of GDS
Neighboring hydrogel particles
Plastic deformation
Slight abrasion
Brittle hydrogel particles
$\sigma_f < \sigma_a$
High degree of disintegration
$\sigma_f > \sigma_a$
No apparent plastic deformation
Low degree of disintegration

Fig. 6

Table 1 Composition of simulated salivary fluid (SSF) and simulated gastric fluid (SGF)

	SSF pH 7.0	**SGF* pH 1.3**
Constituent	Conc. in SSF [g/L]	Conc. in SGF [g/L]
KCl	1.126	0.514
KH_2PO_4	0.503	0.122
$NaHCO_3$	1.142	2.100
NaCl	-	2.760
$MgCl_2(H_2O)_6$	0.030	0.020
$(NH_4)_2CO_3$	0.006	0.074
$CaCl_2(H_2O)_2$	0.221	0.022
α-Amylase	2.530 (150 U/mL)	-
Pepsin	-	5.602 (4000 U/mL)

*6 M HCl solution was used for pH adjustment.

Table 2 Mechanical properties of hydrogel samples

Sample	Concentration (wt%)		Fracture stress (kPa)		Fracture strain (%)	
	Agar	Native gellan gum	Calculated value[1]	Measured value	Calculated value[2]	Measured value
A1.0	1.0	0	23.8	21.1±2.9[a]	25.5	26.5±2.2[a]
A0.7G0.6	0.7	0.6	20.6	23.4±1.6[a]	42.9	37.3±0.6[b]
A0.3G0.9	0.3	0.9	21.9	22.6±1.7[a]	57.4	60.8±1.4[c]
A1.4	1.4	0	43.7	39.6±3.0[b]	28.4	28.9±2.8[a]
A1.1G0.7	1.1	0.7	39.1	40.0±2.2[b]	41.1	38.1±2.2[b]
A0.4G1.1	0.4	1.1	36.0	37.5±1.8[b]	57.9	63.9±2.4[c]
A1.7	1.7	0	62.4	54.1±4.0[c]	29.5	29.7±1.3[a]
A1.6G0.5	1.6	0.5	61.2	56.7±3.6[c]	39.9	41.2±1.9[b]
A0.6G1.5	0.6	1.5	62.9	62.7±6.3[d]	58.2	68.2±1.7[d]
A1.9	1.9	0	76.7	76.1±7.8[e]	33.7	30.6±2.4[a]

All mechanical characteristics were measured at 37 °C with five replications.

[1] Calculated from equation in Fig. S3 (a)

[2] Calculated from equation in Fig. S3 (b)

[a - e] Values with different superscripts are significantly different ($p < 0.05$) within the same groups.

Regarding the sample code, the values after A and G mean the concentrations of agar and native gellan gum, respectively.

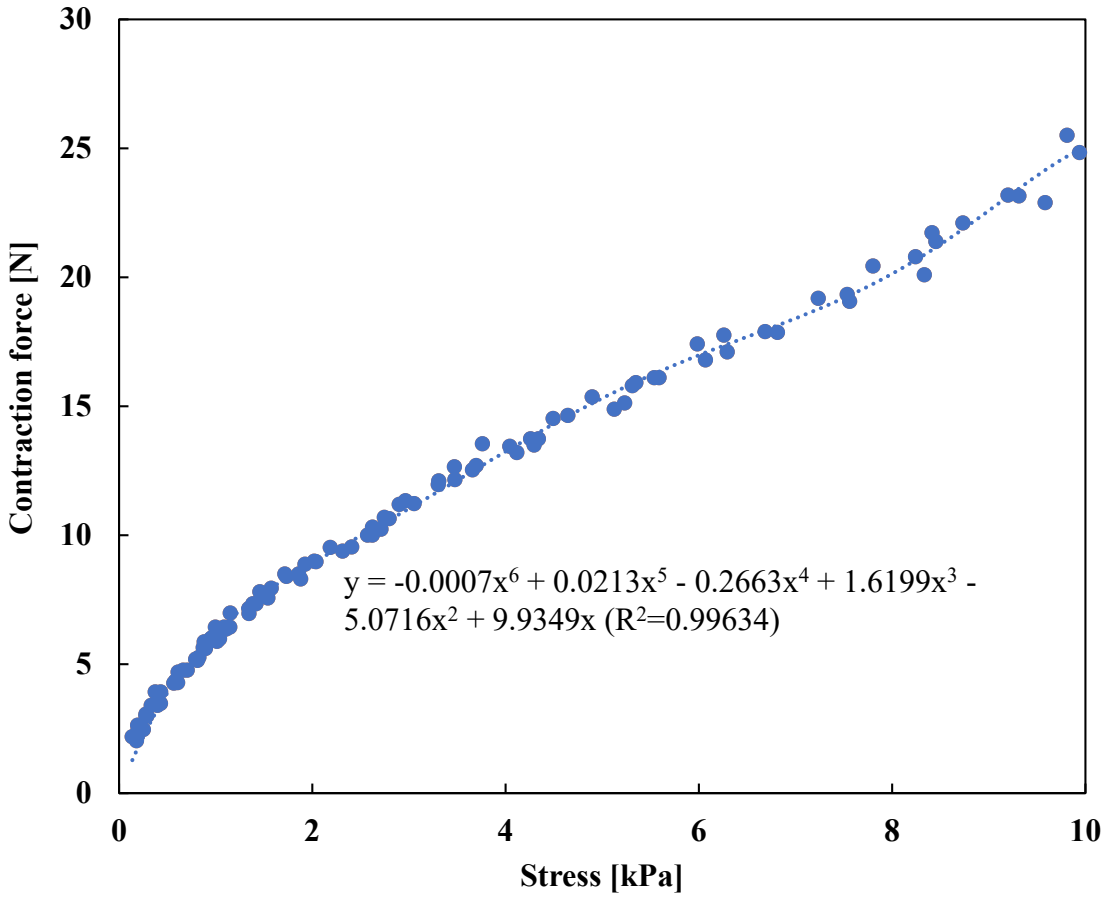

Fig. S1 Correlation between the contraction force of the GDS rollers and the maximum pressure of the balloon

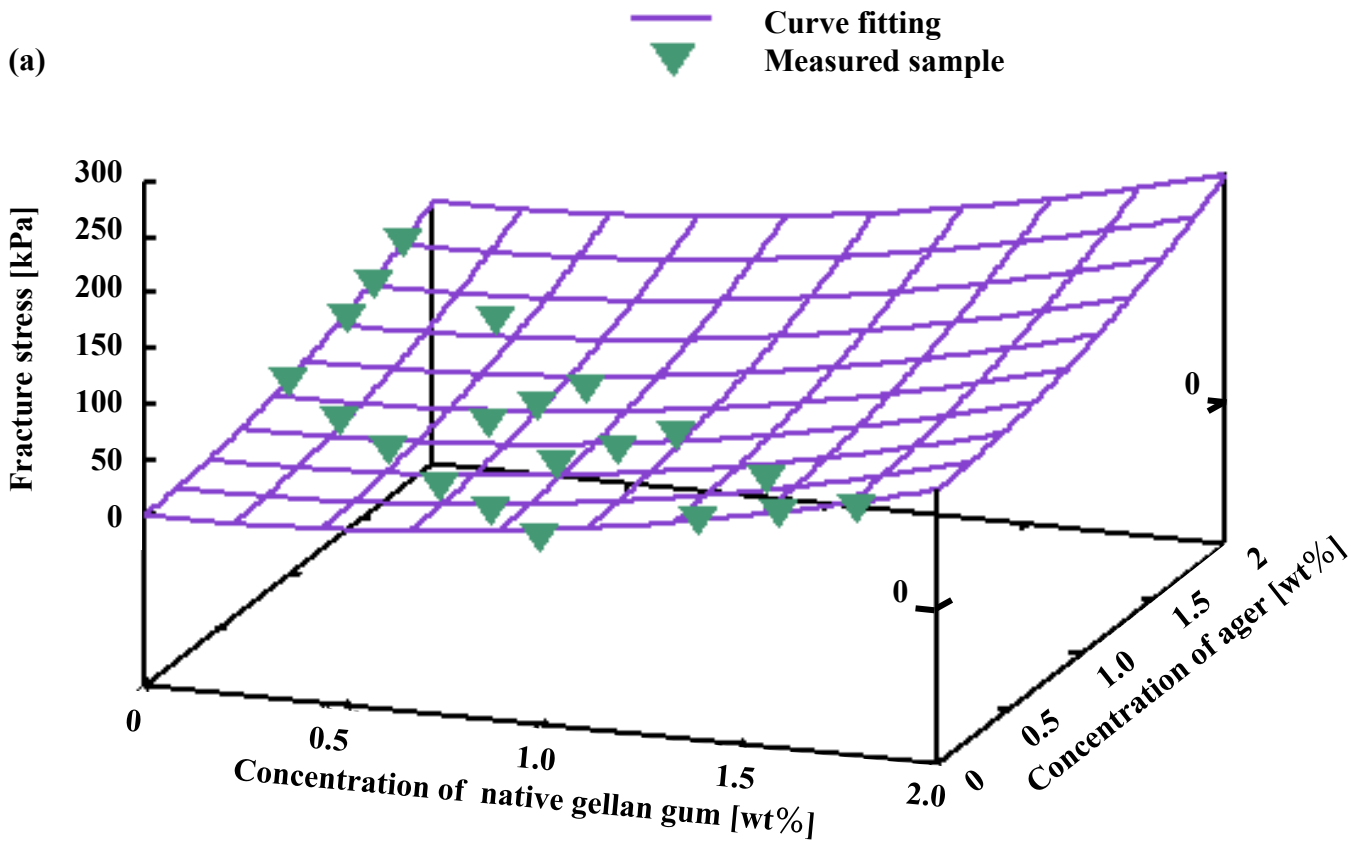

Fracture stress $f_1(x,y)$ $=24.985x^2+18.373y^2+0.403xy-2.31841x+5.453y$
($R^2 = 0.986$)(x: agar concentration; y: native gellan gum concentration)

Fig. S2 Curve fitting of the mechanical properties of each hydrogel sample. (a) Correlation between the concentrations of the two hydrogel agents and fracture stress

(b)

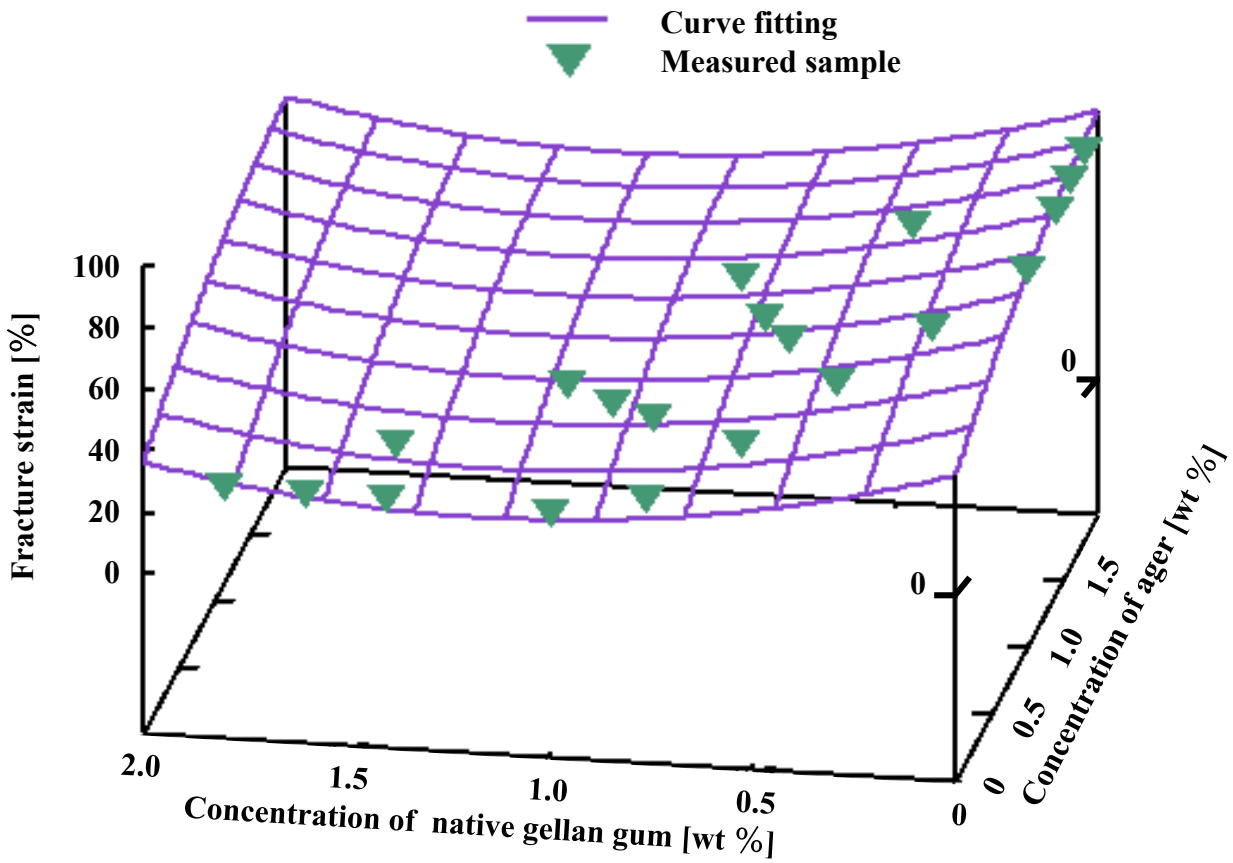

Fracture strain $f_2(x,y)$ $=-5.580x^2+16.656y^2+26.840x-39.227y+48.075$
($R^2 = 0.953$) (x: agar concentration; y: native gellan gum concentration)

(Continues) Fig. S2 Curve fitting of the mechanical properties of each hydrogel sample. (b) Correlation between the concentrations of the two hydrogel agents and fracture strain.

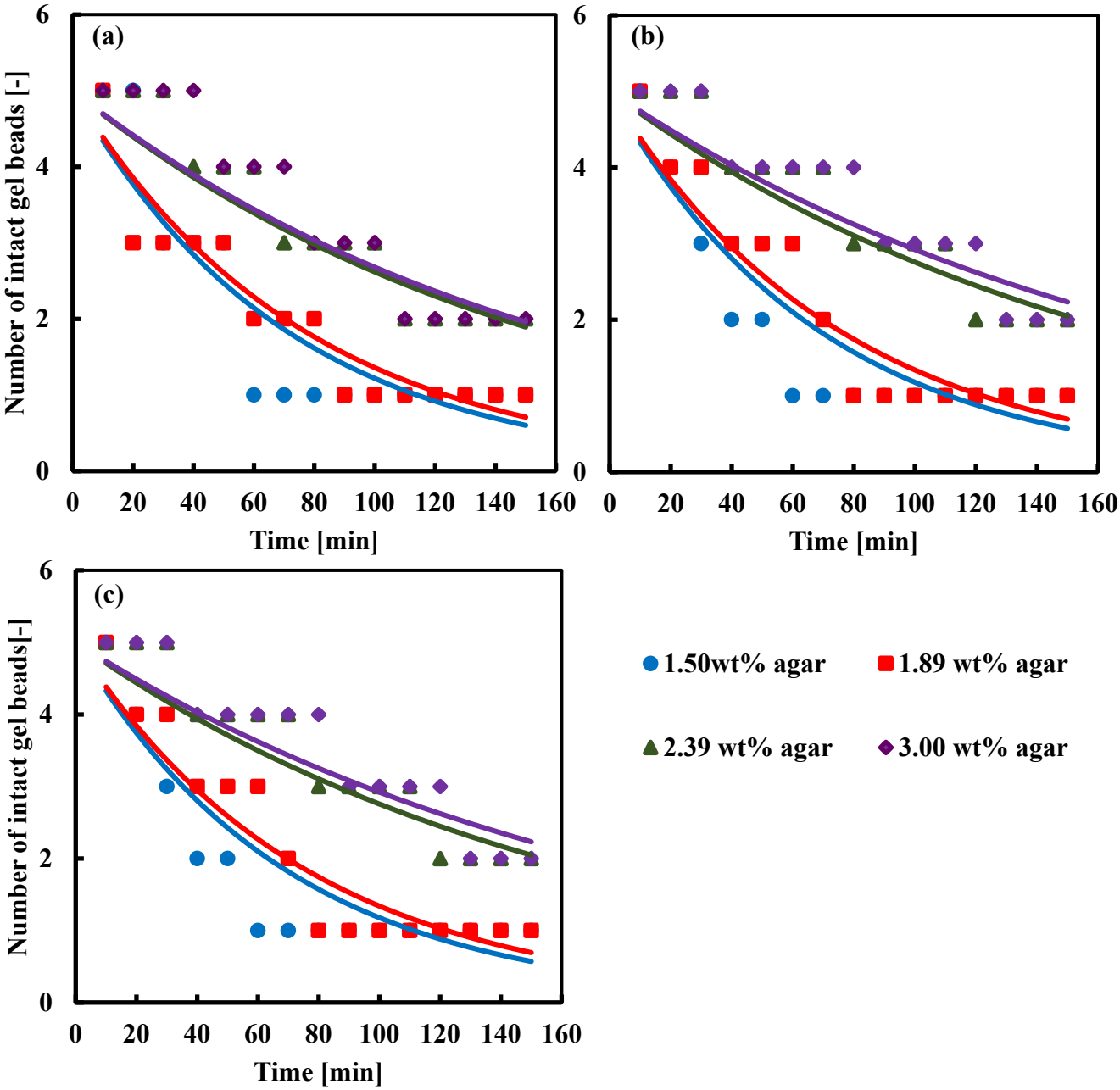

Fig. S3 Time-dependent change of the number of intact agar beads. (a) First, (b) second, and (c) third experiments.

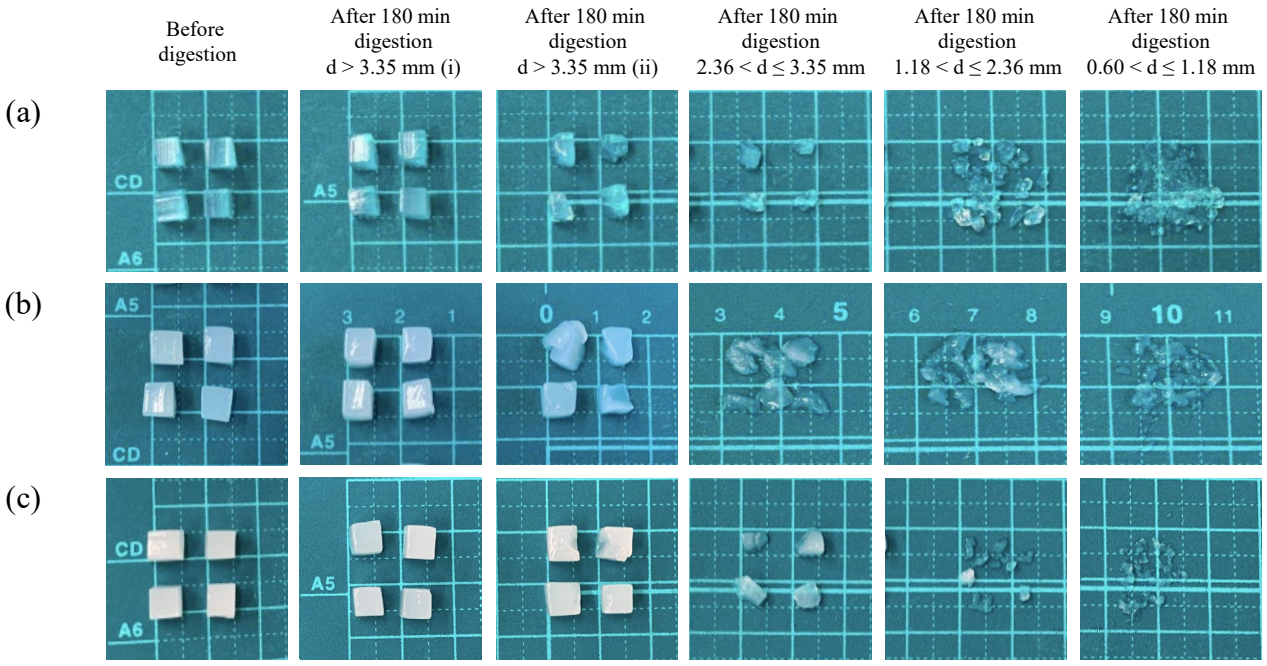

Fig. S4 Photographs showing the examples of the cubes before digestion and after 180 min of digestion. (a) A1.4. (b) A1.1G0.7. (c) A0.4G1.1. (i) Intact hydrogel cubes. (ii) Damaged hydrogel cubes.

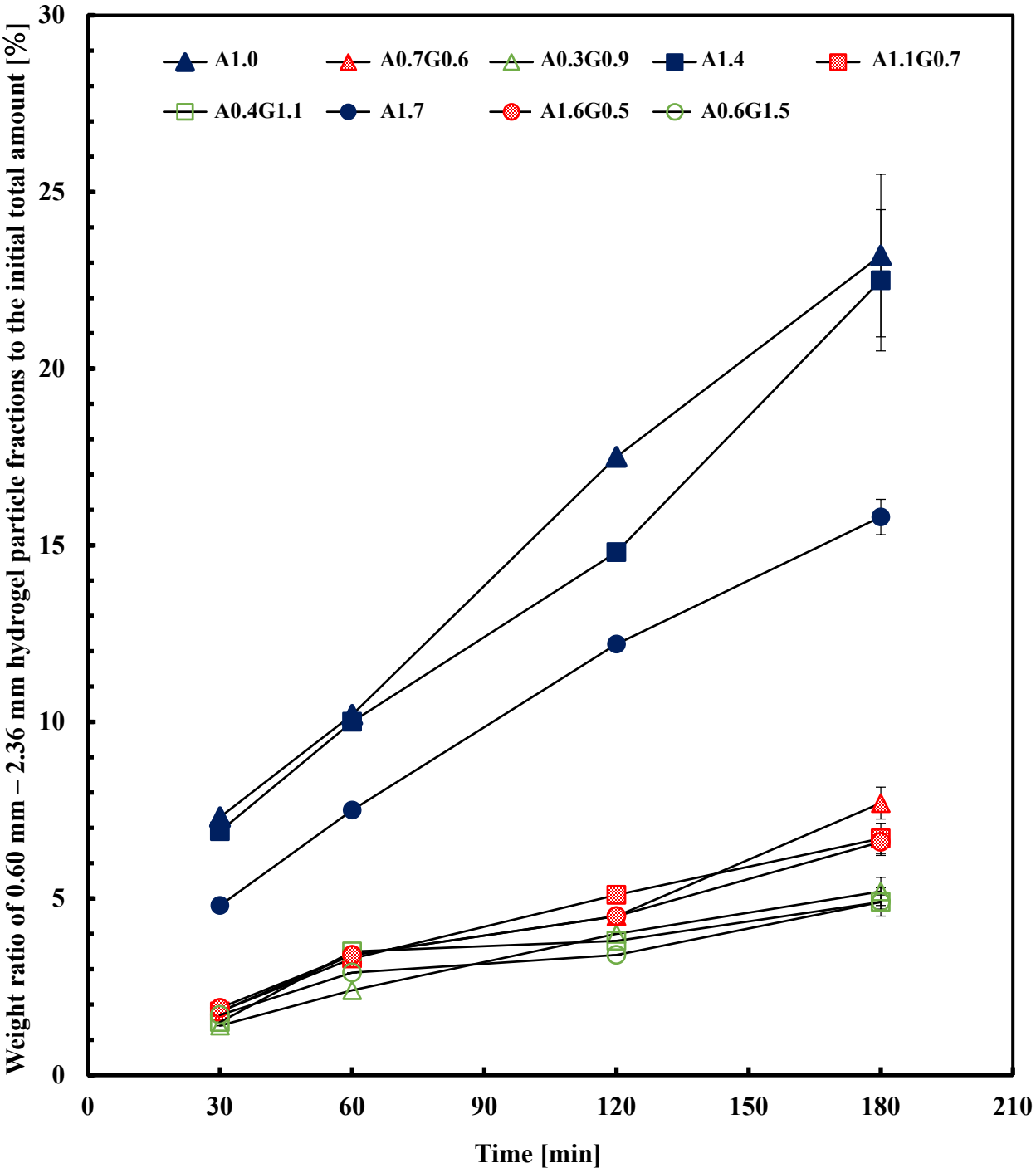

Fig. S5 Weight ratio change of 0.60 mm - 2.36 mm fractions digestion time in the GDS

Table S1 Mechanical properties of the hydrogel samples

Concentration [wt%]		Fracture stress [kPa]		Fracture strain [%]	
Agar	Native gellan gum	Measured value	Calculated value*	Measured value	Calculated value**
1.0	0	24.2	23.8	26.6	25.5
1.4	0	40.7	43.7	27.3	25.8
1.6	0	54.6	55.7	30.2	28.0
1.8	0	70.2	69.3	30.8	31.4
0.8	0.2	17.1	16.7	26.6	32.5
1.4	0.4	50.3	48.5	31.9	35.1
0.6	0.4	16.9	13.0	36.8	40.4
0.8	0.6	22.7	24.3	36.9	40.2
1.0	0.6	29.3	31.1	37.0	40.7
1.1	0.7	36.9	38.9	38.8	41.6
0.4	0.6	11.3	12.8	50.2	49.1
0.6	0.8	23.1	24.7	52.6	49.9
0.6	1.0	33.6	32.0	53.2	50.4
0.7	1.1	43.7	40.4	60.7	50.9
0.2	0.8	15.9	16.0	60.8	58.8
0.4	1.4	51.3	53.0	64.6	63.2
0	1.0	19.8	22.7	72.2	69.3
0	1.4	48.7	45.7	74.1	74.7
0	1.6	63.1	60.2	75.2	76.7
0	1.8	74.0	76.8	76.2	78.3

All mechanical characteristics were measured at 37 ^{o}C with five replications.

* Calculated from equation in Fig. S3 (a)

** Calculated from equation in Fig. S3 (b)